Modeling Multiple Time Scales during Glass Formation with Phase-Field Crystals

Joel Berry and Martin Grant

Physics Department, McGill University, 3600 rue University, Montréal, Québec, Canada H3A 2T8

(Received 8 February 2011; revised manuscript received 1 April 2011; published 29 April 2011)

The dynamics of glass formation in monatomic and binary liquids are studied numerically using a microscopic field theory for the evolution of the time-averaged atomic number density. A stochastic framework combining phase-field crystal free energies and dynamic density functional theory is shown to successfully describe several aspects of glass formation over multiple time scales. Agreement with mode coupling theory is demonstrated for underdamped liquids at moderate supercoolings, and a rapidly growing dynamic correlation length is found to be associated with fragile behavior.

DOI: 10.1103/PhysRevLett.106.175702 PACS numbers: 64.70.Q−, 47.61.−k, 64.70.D−, 81.05.Kf

A unified theoretical framework within which the glass transition may be understood does not currently exist. The most significant theoretical advances have been concentrated near the early stages of slowing, leaving the intermediate and late stages relatively poorly understood. Mode coupling theory (MCT) [1] and molecular dynamics [2], for example, have provided insight into the initial regime of slowing above the so-called crossover temperature T_c, but are ineffective when applied to the slower regimes that occupy roughly 10 orders of magnitude in time between T_c and the glass transition temperature T_g.

Time- or ensemble-averaged dynamic density functional theories (DDFTs) [3–6] have been proposed as a more efficient means of describing slow dynamics below T_c, but several key issues remain unresolved: which of the proposed equations of motion are most appropriate, whether the details of the free energy significantly influence dynamics, and whether the detailed predictions of MCT can be reproduced and eventually improved upon by such theories. Mean-field DFT functionals are known to typically produce multivalley free energy landscapes in which an exponential number of aperiodic solid states coexist below a certain T [7–9]. However, the nature of the transition by which a liquid evolves toward and between these aperiodic solid states upon quenching is influenced heavily by the microscopic dynamics and thus, in DDFT, the equation of motion employed. Approximate analytic results [5] indicate that two DDFT equations of motion may describe a MCT-type glass transition, but numerical simulations have confirmed only stretched exponential decay and super-Arrhenius slowing in related, non-DDFT models [4]. Here we provide direct numerical solutions for a candidate DDFT that considers both inertia and damping, and utilizes the simplest DFT free energy, the phase-field crystal (PFC) class [10].

The dimensionless Helmholtz potential of a two component PFC system can be written [11]

$$F = \int d\vec{r}[f_A + f_B + f_{AB}], \tag{1}$$

where

$$f_i = \frac{n_i}{2}[B_i^\ell + (q_i^2 + \nabla^2)^2]n_i - \frac{w_i}{3}n_i^3 + \frac{u_i}{4}n_i^4 + H_i(|n_i|^3 - n_i^3)$$

and

$$f_{AB} = \frac{n_A}{2}(q_{AB}^2 + \nabla^2)^2 n_B + \frac{\lambda_1}{2}n_A^2 n_B^2 + \frac{\lambda_2}{2}(\nabla\delta c)^2.$$

In this notation $i = A$ or B, $n_i = n_i(\vec{r}, t) + \bar{n}_i$ is the scaled time-averaged number density of i particles, $\bar{n}_i$ is the species average number density, B_i^ℓ is related to the liquid bulk modulus, q_i sets the equilibrium distance between particles of the same species, q_{AB} sets that between A and B particles, and w_i, u_i, H_i, λ_1, and λ_2 are constants (see Ref. [10] for further discussion of how these parameters relate to material properties). The terms multiplied by H_i discourage $n_i < 0$ and are the distinguishing feature of the vacancy or VPFC model [11]. A hard $n_i \geq 0$ cutoff enforces the physical interpretation of n_i as a number density and in doing so produces a range of nonlinear responses. The resulting solutions take the form of interacting time-averaged density peaks, with local regions of $n_i \simeq 0$ representing unoccupied, or vacancy, sites.

The simplest dynamics conserving n_i may be written

$$\frac{\partial n_i}{\partial t} = \nabla^2 \frac{\delta F}{\delta n_i} + \sqrt{D_i}\eta_i, \tag{2}$$

where t is dimensionless time, $D_i \sim T$, and η_i is a Gaussian stochastic noise variable with $\langle \eta_i(\vec{r}_1, t_1)\eta_i(\vec{r}_2, t_2)\rangle = \nabla\cdot\nabla\delta(\vec{r}_1 - \vec{r}_2)\delta(t_1 - t_2)$. A second option is the overdamped equation of DDFT,

$$\frac{\partial n_i}{\partial t} = \nabla\cdot\left(n(\vec{r}, t)\nabla\frac{\delta F}{\delta n_i}\right) + \sqrt{D_i}\nu_i, \tag{3}$$

where $n(\vec{r}, t)$ is generally set to $n_i(\vec{r}, t)$ and $\langle \nu_i(\vec{r}_1, t_1)\nu_i(\vec{r}_2, t_2)\rangle = \nabla\cdot\nabla[n(\vec{r}, t)\delta(\vec{r}_1 - \vec{r}_2)\delta(t_1 - t_2)]$. A third equation reintroduces some of the faster dynamics by also including an inertial or wavelike term,

$$\frac{\partial^2 n_i}{\partial t^2} + \beta_i \frac{\partial n_i}{\partial t} = \alpha_i^2 \nabla \cdot \left(n(\vec{r}, t) \nabla \frac{\delta F}{\delta n_i} \right) + \sqrt{D_i} \nu_i, \quad (4)$$

where α_i and β_i are constants [12].

Previous PFC simulations indicate that Eq. (2) supports metastable glassy states but in general produces a discontinuous, nucleation driven liquid to glass transition [9]. Recent analyses of Eqs. (3) and (4) suggest that both may recover the class of MCT equations for the liquid dynamic correlators that successfully describe a wide range of glass forming behaviors [5]. Here we numerically investigate, without approximation, Eq. (4) with $n(\vec{r}, t) = 1$, where the inclusion of stochastic noise implies a time-averaged rather than ensemble-averaged interpretation of DDFT [13]. Equilibrium liquid states at high D_i were quenched by lowering the stochastic noise amplitude $T = T_0 D_i$ at a rate $\dot{T}$, and the freezing transition was analyzed for onset of vitrification or crystallization.

We begin with results for monatomic systems, outlined in Fig. 1. For $T \gtrsim 1.6$ the structure and dynamics are those of a normal liquid. The measured intermediate scattering functions $[F_{ij}(q, t) = \langle \delta n_i(q, 0) \delta n_j^*(q, t) \rangle / F_{ij}(q, 0)]$ decay exponentially, the corresponding average relaxation times show an Arrhenius T dependence, and the structure factors are characteristic of an equilibrium liquid state. The function $S^P(q)$ quantifies the structural correlations of the localized peaks in the density field. We define $S_{ij}^P(q) = \langle \delta n_i^P(q) \delta n_j^{P*}(q') \rangle$, where $\delta n_i^P(r)$ is a binary map of the positions of the local number density peaks.

Below $T \simeq 1.6$, the liquid begins to show signs of non-equilibrium behavior and the onset of glass formation. $F(q, t)$ becomes increasingly stretched and begins to exhibit a shoulder, the average relaxation time briefly begins to grow with a super-Arrhenius T dependence, and a split second peak emerges in $S^P(q)$. But signs of glass formation persist only to the freezing temperature of the crystal, T_f. Below this point crystallization interrupts the apparent glass transition unless the liquid is rapidly quenched well below T_f. The time-temperature-transformation (TTT) diagram shown in Fig. 1(d) demonstrates this behavior. The profile of the nose feature is typical for materials with relatively marginal glass forming ability, such as metallic glasses. Since long-lived glassy states are not supported in the region $0.6 \lesssim T \lesssim T_f$, one cannot study a gradual dynamic transition from liquid to glass. This behavior is expected for simple monatomic systems.

Thus we proceed to binary liquids and outline in Fig. 2 the qualitative behavior of one such model system for a range of dynamic conditions, from highly underdamped ($\alpha_i/\beta_i = 100$) to highly overdamped ($\alpha_i/\beta_i = 0.01$). The chosen model contains equal number densities of A and B atoms ($\bar{n}_A = \bar{n}_B = 0.075$), and the equilibrium spacing of A atoms is 20% smaller than that of B atoms ($R_A/R_B = q_B/q_A = 0.8$). Only the NN correlations are plotted in Figs. 2(a)–2(c), where N denotes the full density field $n_A + n_B$. When damping dominates, an effectively stable glass with dynamics resembling those of a strong glass former is generated. The dynamic correlators are generally best fit as a single exponential decay for all accessible T, with increased stretching as T is lowered, but any plateaus are absent or ill-defined in the $\alpha_i/\beta_i \lesssim 1$ data. The relaxation times exhibit a nearly Arrhenius T dependence over the entire accessible T range.

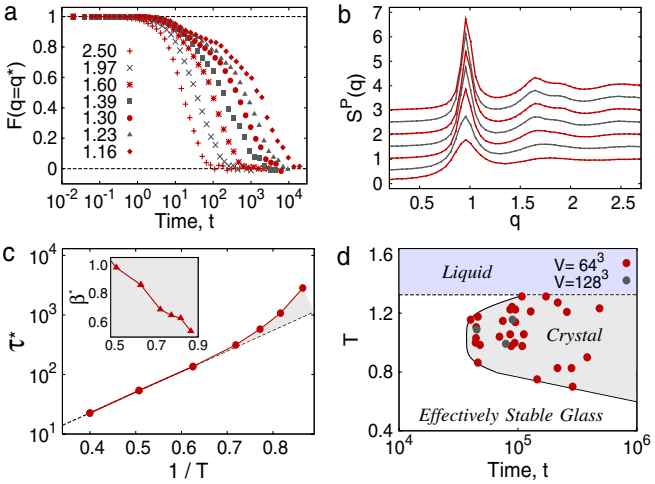

FIG. 1 (color online). Glass formation and crystallization in the monatomic VPFC model. (a) $F(q^*, t)$ at various T where q^* corresponds to the first peak maximum in $S^P(q)$, (b) $S^P(q)$ at same T as in (a), offset vertically by $0.5n$ with $n = 0, 1, \ldots,$ (c) Arrhenius plot of τ^* from $F(q^*, t)$, (inset) stretching exponent β^* from fit to $F(q^*, t) = \exp[-(t/\tau^*)^{\beta^*}]$, (d) TTT diagram: quenches from $T = 1.6$ at various $\dot{T}$, points denote where crystallization occurred. $\bar{n}_A = 0.15$, $B_A^\ell = -0.9$, $q_A = 1$, $w_A = 0$, $u_A = 1$, $H_A = 1500$, $T_0 = 1000$, $\alpha_A = 1$, $\beta_A = 0.01$, $f_B = f_{AB} = 0$, $\Delta x = 1.0$, $\Delta t = 0.02$, $V = 128^3$.

At the opposite extreme, when inertia dominates, a transition with dynamics characteristic of fragile liquids is generated. The dynamic correlators show both stretching and clear plateauing as T is lowered, and the divergence of the relaxation time is well fit by the Vogel-Fulcher form $[\tau = A \exp[B/(T - T_0)]]$. This divergence becomes increasingly super-Arrhenius at higher T as α_i/β_i grows. The underdamped transition at this level of detail qualitatively resembles that described by MCT.

The fragility of the PFC liquid therefore appears to be strongly linked with the balance of inertial and damping terms in Eq. (4), α_i/β_i. The degree of fragility is in turn correlated with the nominal spatial extent of cooperative dynamic behavior, which is set by an inherent length scale associated with the inertial term. This term generates wave modes which propagate over a fixed length scale in a crystal before being damped, and the resulting dynamic correlation length follows $\xi_D^{\text{crystal}} \sim \alpha_i/\beta_i$ [12]. In a normal liquid these correlations are largely suppressed by the low density and weak structural correlations, so that $\xi_D^{\text{liquid}} \ll \xi_D^{\text{crystal}}$. But with greater supercooling, as the system becomes increasingly dense and solidlike, the inertial correlations survive over length scales which likely

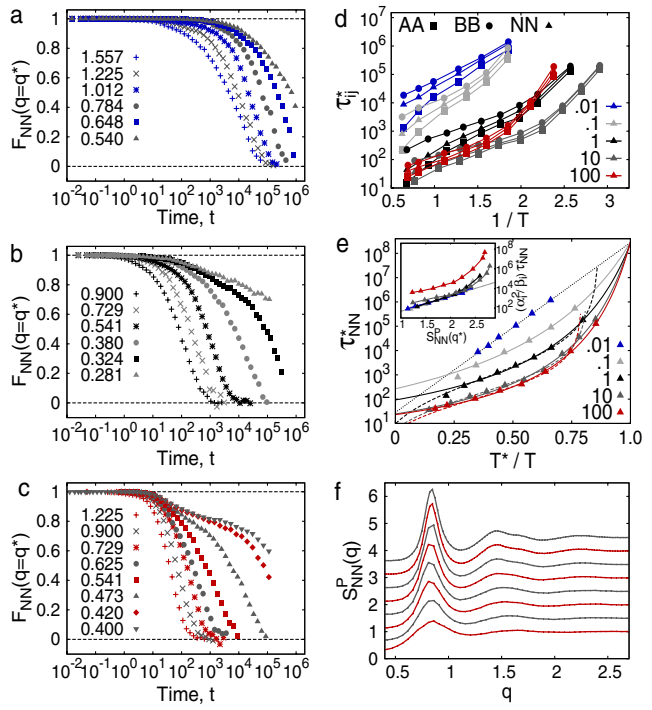

FIG. 2 (color online). Binary VPFC results for various damping conditions. $F_{NN}(q^*, t)$ at various T shown for α_i/β_i of (a) 0.01, (b) 1, and (c) 100. (d) Arrhenius plot of the structural relaxation times τ^*_{ij}, (e) the same data (NN only) scaled to clarify strong versus fragile behaviors, with Vogel-Fulcher fits shown as solid lines and power law fits as dashed lines. Inset: $(\alpha_i^2/\beta_i)\tau^*_{NN}$ vs $S^P_{NN}(q^*)$, demonstrating deviation from scaling when inertial effects become large. (f) $S^P_{NN}(q)$ for $\alpha_i/\beta_i = 100$. $\bar{n}_A = \bar{n}_B = 0.075$, $B^\ell_i = -0.9$, $q_A = 1$, $q_B = 0.8$, $w_i = 0$, $u_i = 1$, $H_i = 1500$, $T_0 = 1000$, $q_{AB} = 8/9$, $\lambda_1 = 100$, $\lambda_2 = 0$, $\Delta x = 1.0$, $\Delta t = 0.025$, $V = 64^3$, 128^3, or 256^3.

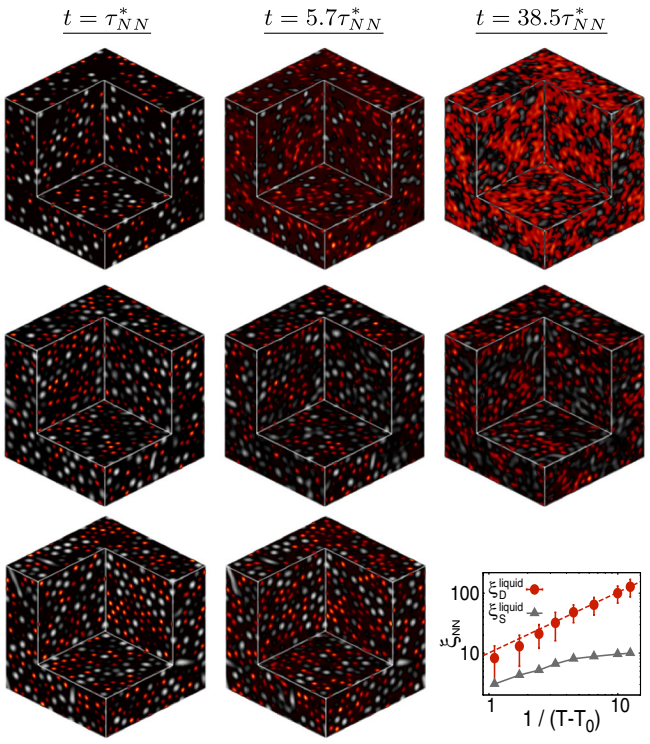

FIG. 3 (color online). Time-averaged density evolution in the supercooled binary liquid with $\alpha_i/\beta_i = 100$. $N(\vec{r})$ at $T = 1.225$ (top), 0.541 (middle), and 0.420 (bottom) averaged over the indicated multiples of each system's τ^*_{NN}. A subcubic section of each cell has been removed to reveal a portion of the inner simulation. $n_A(\vec{r})$ time averages are black and gray (orange), $n_B(\vec{r})$ time averages are black and white. Bottom right: Log plot of static and dynamic correlation lengths versus $1/(T - T_0)$. The dashed red line has a slope of 1.0.

approach ξ_D^{crystal}. Roughly, $\xi_D^{\text{liquid}} \to \xi_D^{\text{crystal}} \sim \alpha_i/\beta_i$ as $T \to T_g$ [14].

The effects of this growing dynamic length scale are therefore especially prominent in highly underdamped systems, where its properties can be observed and quantified through finite size effects in $F(q, t)$. For example, when $\alpha_i/\beta_i = 100$ finite size effects become numerically insurmountable below $T \simeq 0.4$. Measurements indicate that the average two point liquid static correlation length ξ_S^{liquid} grows slowly, approximately as $1/T$, while the dynamic correlation length grows more rapidly, as $\xi_D^{\text{liquid}} \sim (T - T_0)^{-1\pm0.35}$ (see Fig. 3). This indicates that the supercooled liquid exhibits heterogeneous dynamics driven by strong inertial effects. Similar links between slowing dynamics and growing dynamic correlation lengths have been widely discussed [2,8,15–18].

A correlation between fragility and the length scale for cooperativity is consistent with existing interpretations of strong and fragile liquids [19]. We also find a relevant link to recent experiments on colloidal glasses which demonstrate a transition from strong to fragile behavior as the elastic properties of the colloidal particles become increasingly stiff [20]. When overdamped, Eq. (4) describes a very soft, viscoelastic solid, while elastic stiffness and fragility both increase as damping is reduced. This is because $\alpha_i \sim v_s \sim \sqrt{E}$, where v_s is a sound speed and E is the relevant elastic modulus. Greater elastic stiffness should therefore correspond to reduced effective damping and, we expect, increased fragility [21]. This agrees with the trend found in Ref. [20].

Figure 3 shows simulation images of $N(\vec{r})$ for the $\alpha_i/\beta_i = 100$ system averaged over various times at $T = 1.225$, 0.541, and 0.420. Caging is apparent at short times for all T, but the long time averages at low T retain more of their original structure as the peaks exhibit less translational freedom. It is important to note that time averages are shown at equal multiples of each liquid's relaxation time, not at equal t, so that time scales remain normalized as T is varied. The continuous but rapid decline in translational freedom as T is lowered signals a smooth transition from liquidlike to activated dynamics. This is consistent with the postulated crossover at T_c, below which relaxations are expected to be limited by increasingly rare, heterogeneously correlated cage escape events. This transition coincides with the emergence of the plateau in

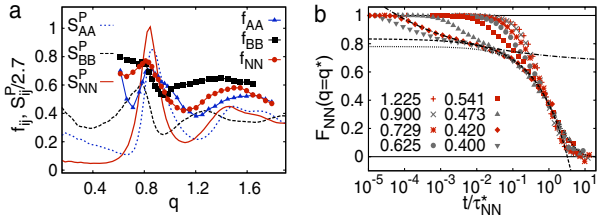

FIG. 4 (color online). The highly underdamped $\alpha_i/\beta_i = 100$ model and MCT. (a) $f_{ij}(q)$ and $S^P_{ij}(q)/2.7$ at $T = 0.420$, (b) $F_{NN}(q, t/\tau^*_{NN})$ with various MCT scaling functions. Dashed line: von Schweidler power law; dotted line: stretched exponential; Dash-dotted line: critical decay power law.

$F_{ij}(q, t)$ and the split second peak in $S^P_{NN}(q)$ below $T \simeq 0.6$, as shown in Fig. 2.

Figure 4 shows data for the $\alpha_i/\beta_i = 100$ system relevant for comparison with the predictions of MCT. The nonergodicity parameter, $f_{ij}(q)$ [height of the plateau in $F_{ij}(q, t)$], is plotted in Fig. 4(a) for $T = 0.420$. It follows the normal MCT behavior in which f_{ij} decays while oscillating in phase with $S_{ij}(q)$. Some of the dynamic scaling behaviors predicted by MCT are tested in Fig. 4(b). Present results indicate that the von Schweidler scaling for late β relaxations (initial decay after plateau), $F(q, t) = f - B(t/\tau)^b$, is obeyed reasonably well over 2–3 orders of magnitude in time. The measured exponent $b \simeq 0.45 \pm 0.15$ is comparable to typical values. Fits to the MCT critical decay power law (initial decay to plateau), $F(q, t) = f + At^{-a}$, give $a \simeq 0.3 \pm 0.1$.

The late α relaxations predicted by MCT are generally well approximated by a stretched exponential decay. Our data are fit quite well by this form, as shown in Fig. 4(b), but with a stretching exponent β that decreases with T from approximately 1 to 0.6. MCT also predicts that the initial divergences of the fast and slow relaxation times follow power laws, $\tau_\beta \sim (T - T_c)^{-1/(2a)}$ and $\tau_\alpha \sim (T - T_c)^{-\gamma}$, respectively, where $\gamma = 1/(2a) + 1/(2b)$. Fits to these forms are shown in Fig. 2(e), and though the Vogel-Fulcher fits are superior, the power laws are reasonably accurate through the early super-Arrhenius growth.

These results confirm that the DDFT equation of motion with inertia does in fact describe a glass transition, and that when damping is weak this transition strongly resembles both the structural glass transition observed for fragile glass formers as well as that predicted by MCT. Our results are consistent with a picture in which fragility is driven by a large dynamic correlation length, which in some cases can be associated with large elastic moduli. A direct test of this association could be performed using colloidal systems such as those of Ref. [20]. By varying the degree of confinement, one could compare the relative magnitudes and growth rates of any dynamic correlation length as behavior is varied from strong to fragile.

The authors acknowledge valuable comments from Ken Elder and Dan Vernon, and support from the Natural Science and Engineering Research Council of Canada, le Fonds Québécois de la recherche sur la nature et les technologies, and the Schulich and Carl Reinhardt Endowments. Simulations were performed on a CLUMEQ/Compute Canada cluster at the Université Laval and a Beowulf cluster at McGill University.

[1] W. Götze, *Complex Dynamics of Glass-Forming Liquids: A Mode-Coupling Theory* (Oxford University Press, Oxford, England, 2009).
[2] S. C. Glotzer, J. Non-Cryst. Solids **274**, 342 (2000).
[3] U. M. B. Marconi and P. Tarazona, J. Chem. Phys. **110**, 8032 (1999); A. J. Archer and R. Evans, J. Chem. Phys. **121**, 4246 (2004).
[4] K. Fuchizaki and K. Kawasaki, J. Phys. Condens. Matter **14**, 12 203 (2002); L. M. Lust, O. T. Valls, and C. Dasgupta, Phys. Rev. E **48**, 1787 (1993).
[5] A. Andreanov, G. Biroli, and A. Lefèvre, J. Stat. Mech. (2006) P07008; B. Kim and K. Kawasaki, J. Phys. A **40**, F33 (2007); A. J. Archer, J. Chem. Phys. **130**, 014509 (2009); A. J. Archer, J. Phys. Condens. Matter **18**, 5617 (2006).
[6] U. M. B. Marconi and P. Tarazona, J. Chem. Phys. **124**, 164901 (2006); U. M. B. Marconi and S. Melchionna, J. Chem. Phys. **126**, 184109 (2007).
[7] Y. Singh, J. P. Stoessel, and P. G. Wolynes, Phys. Rev. Lett. **54**, 1059 (1985); C. Dasgupta and S. Ramaswamy, Physica (Amsterdam) **186A**, 314 (1992).
[8] V. Lubchenko and P. G. Wolynes, Annu. Rev. Phys. Chem. **58**, 235 (2007).
[9] J. Berry, K. R. Elder, and M. Grant, Phys. Rev. E **77**, 061506 (2008).
[10] K. R. Elder and M. Grant, Phys. Rev. E **70**, 051605 (2004); K. R. Elder, N. Provatas, J. Berry, P. Stefanovic, and M. Grant, Phys. Rev. B **75**, 064107 (2007).
[11] P. Y. Chan, Ph.D. thesis, Univeristy of Illinois at Urbana-Champaign, 2007; P. Y. Chan, N. Goldenfeld, and J. Dantzig, Phys. Rev. E **79**, 035701(R) (2009).
[12] P. Stefanovic, M. Haataja, and N. Provatas, Phys. Rev. Lett. **96**, 225504 (2006).
[13] A. J. Archer and M. Rauscher, J. Phys. A **37**, 9325 (2004);.K. Kawasaki, Physica (Amsterdam) **362A**, 249 (2006).
[14] This behavior may signal the onset of a percolation-type transition, wherein the growing correlation volumes eventually form a continuous rigid network persisting over all accessible t. See, for example, J. C. Conrad *et al.*, Phys. Rev. Lett. **97**, 265701 (2006); S. A. Baeurle, A. Hotta, and A. A. Gusev, Polymer **47**, 6243 (2006) or Ref. [8].
[15] J. H. Gibbs and E. A. di Marzio, J. Chem. Phys. **28**, 373 (1958); G. Biroli and J. P. Bouchaud, J. Phys. Condens. Matter **19**, 205101 (2007).
[16] H. Tanaka *et al.*, Nature Mater. **9**, 324 (2010).
[17] K. Kim and R. Yamamoto, Phys. Rev. E **61**, R41 (2000).
[18] E. R. Weeks *et al.*, Science **287**, 627 (2000); C. R. Nugent *et al.*, Phys. Rev. Lett. **99**, 025702 (2007).
[19] C. A. Angell *et al.*, J. Appl. Phys. **88**, 3113 (2000).
[20] J. Mattsson *et al.*, Nature (London) **462**, 83 (2009).
[21] Links between fragility and elastic properties have also been discussed in V. N. Novikov, Y. Ding, and A. P. Sokolov, Phys. Rev. E **71**, 061501 (2005).